

---

# FISHER INFORMATION IMPROVED TRAINING-FREE CONDITIONAL DIFFUSION MODEL

---

Kaiyu Song, Hanjiang Lai  
Sun Yat-Sen University  
{songky7, laihanj3}@mail2.sysu.edu.cn

## ABSTRACT

Recently, the diffusion model with the training-free methods has succeeded in conditional image generation tasks. However, there is an efficiency problem because it requires calculating the gradient with high computational cost, and previous methods make strong assumptions to solve it, sacrificing generalization. In this work, we propose the Fisher information guided diffusion model (FIGD). Concretely, we introduce the Fisher information to estimate the gradient without making any additional assumptions to reduce computation cost. Meanwhile, we demonstrate that the Fisher information ensures the generalization of FIGD and provides new insights for training-free methods based on the information theory. The experimental results demonstrate that FIGD could achieve different conditional generations more quickly while maintaining high quality.

## 1 Introduction

The diffusion models (DMs) [1] make great success in image generation tasks, outperforming previous generative models like GANs [2]. It is natural to use the diffusion model to achieve various downstream tasks [3, 4, 5]. One popular area is conditional generation [6, 7, 8], where conditions are added to guide the generative model to produce desired images, such as text [9, 10, 11], face ID [4, 7, 12], and style images [13]. These methods mainly contain two categories: training-based methods [9, 7] and training-free methods [6, 14, 15].

Training-free methods aim to use the DMs to solve different tasks without extra training. Given the condition  $c$ , one popular method is to sample from the posterior distribution  $p(\mathbf{x}|c)$  by incorporating the gradient of the log likelihood  $\nabla_{\mathbf{x}} \log p(\mathbf{x}|c)$  [6]. The likelihood term could be formulated as the unconditional term  $\nabla_{\mathbf{x}} \log p(\mathbf{x})$  and conditional term  $\nabla_{\mathbf{x}} \log p(c|\mathbf{x})$  by the Bayesian rule [6].

The unconditional term is equal to the score function [16] learned by the DMs. The conditional term seems analytically intractable in terms of the DMs, due to their dependence on time  $t$ . To decouple the dependence, Chung *et al.* [6] used the estimation  $\hat{\mathbf{x}}_{0|t}$  [17] of  $\mathbf{x}$ , where  $\hat{\mathbf{x}}_{0|t}$  actually is the final state of  $\mathbf{x}$  by  $t \rightarrow 0$ . In this way, for different tasks, we only need to define a differentiable metric to sample from  $\log p(c|\hat{\mathbf{x}}_{0|t})$  by incorporating the gradient  $\nabla_{\mathbf{x}} \log p(c|\hat{\mathbf{x}}_{0|t})$ . The metric could be the distance norm [6, 14, 15, 18] and an energy function [4].

There are two partial parts for calculating  $\nabla_{\mathbf{x}} \log p(c|\hat{\mathbf{x}}_{0|t})$  [6] (More details can be found in Sec. 3): 1) The gradient of the metric itself. 2) The gradient of  $\hat{\mathbf{x}}_{0|t}$ . This causes the computation cost and limits the applications of the training-free method since we need to calculate the gradient of the UNet of DMs first in order to calculate the gradient of  $\hat{\mathbf{x}}_{0|t}$ . He *et al.* [15] introduced the manifold theory based on the linear manifold hypothesis [15, 18] to avoid calculating the gradient of  $\hat{\mathbf{x}}_{0|t}$  based on the inverse problem [19].

The linear manifold hypothesis is a strong assumption, requiring a specific metric design, and limiting its generalization. Besides, we lack the interpretation of the behavior of  $\nabla_{\mathbf{x}} \log p(c|\hat{\mathbf{x}}_{0|t})$  based on the manifold theory, which hinders further improvement.

To alleviate these problems, we propose the Fisher information guided diffusion model (FIGD). Concretely, FIGD first introduces the Fisher information [20] to interpret  $\nabla_{\mathbf{x}} \log p(c|\hat{\mathbf{x}}_{0|t})$ . Then, by leveraging the central limited theorem [20], FIGD estimates it based on the Cramér-Rao bound and proposes a simple yet effective method to generate high-quality images without any additional assumption. In the end, based on the view of the information

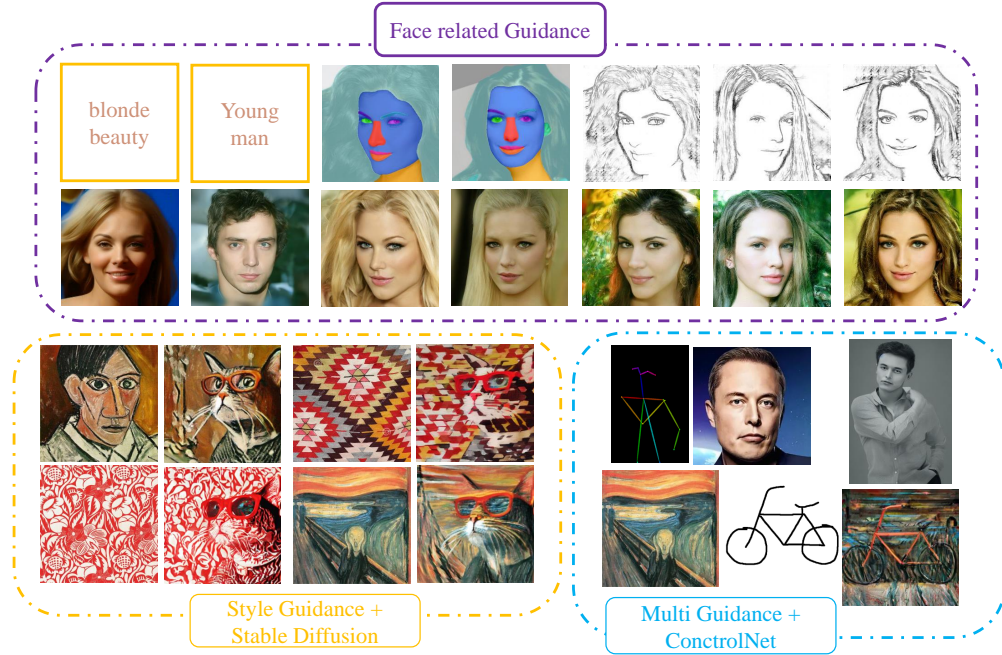


Figure 1: FIGD controls the generation of the diffusion in a training-free way. We demonstrate some applications FIGD supports. In the face-related guidance, we first use text prompts as guidance to generate prompt-related faces. Then, we use face segmentation and sketches as the guidance respectively. In the stable diffusion based tasks, we use prompt: "a cat wearing glasses" with a style image to guide the generation process. In ControlNet related tasks, we first use pose maps and an additional face ID with "young man, realistic photo" text prompt as the guidance. Then, we use the sketch, "bike" text prompt, and the additional style image as the guidance.

theory,  $\nabla_{\mathbf{x}} \log p(c|\hat{\mathbf{x}}_{0:t})$  could be interpreted as accumulating the information following the direction of the guidance. This keeps the generalization of FIGD and also explains the expertise that remained from previous work. Experimental results show that FIGD achieves state-of-the-art (SOTA) results in various downstream tasks.

To sum up, the main contributions of this paper are:

- We propose FIGD, the Fisher information guided diffusion model framework. There is no additional assumption of FIGD, where we could directly design a differentiable metric to achieve various downstream tasks without limitations.
- Fisher information provides a new insight into training-free methods. This helps us explain the behavior of the log likelihood and some expertise remains from previous work.
- The experimental shows that FIGD could be 2x speedups compared with SOTA methods in some conditions while maintaining high quality.

## 2 Related Work

**Training-based methods.** These methods aim to fine-tune the parameters of the DMs based on different downstream tasks. For example, DreamBooth [21] fine-tuned the UNet of the diffusion model to inject the new concept. ControlNet [7] introduced an additional UNet and fine-tuned it while freezing the original UNet. Stable Diffusion [9] introduced the transformer layers to fuse with the text embedding. Training-based methods could generate high-quality images related to the condition but the cost is too high since it needs to fine-tune each time for different downstream tasks.

**Training-free methods.** Some training-free methods focus on the structure and potential of the UNet. For example, Tumanyan *et al.* [13] leveraged the attention maps from attention layers. Jaeseok *et al.* [3] found the "h-space" among the UNet of the diffusion model. Wu *et al.* [22] directly changed the inputs of the UNet. Except for the success, these methods need a special design based on the downstream tasks and thus limit their generalization.

The other methods [6, 14, 4] focus on sampling from the posterior distribution. For example, DPS [6] first used the distance norm as the metric based on the inverse problem. FreeDom [4] further used the energy function as the metric, which extended it from solving the inverse problem to more widely downstream tasks such as face ID generation[23]. He *et al.*[15] introduced the manifold hypothesis based on the inverse problem and decreased the computation cost. However, there is a strong assumption of the manifold hypothesis.

**Information theory with the DMs.** In light of the SDE [16] that introduced the score function to explain the behavior of DMs, as one of the important tools, information theory shows the potential to further open the black box and make further improvements. Both information theoretical diffusion [24] and InforDiffusion [25] leveraged mutual information to interpret the correlation behind the observed and hidden variables to improve the quality of the generation quality. Interpretable diffusion [26] further explained what is the most important part of the input for DMs similar to CAM [8]. In this paper, we remove the assumption of the manifold hypothesis and offer a new view to interpret the behavior of the gradient based on the information theory.

### 3 Preliminary

**Problem definition.** Given a pre-trained diffusion model, the outputs could be defined as  $\epsilon_\theta(\mathbf{x}_t, t)$ , where  $\epsilon_\theta(*, *)$  is the score function [16] based on the UNet with the set of parameters  $\theta$ ,  $\mathbf{x}_t$  is the state in the  $t$ -th timestep [1], the reverse process could be defined as:

$$\mathbf{x}_{t-1} = (1 + 0.5\beta_t)\mathbf{x}_t + \beta_t \underbrace{\nabla_{\mathbf{x}_t} \log p(\mathbf{x}_t)}_{\epsilon_\theta(\mathbf{x}_t, t)} + \sqrt{\beta_t}\epsilon, \quad (1)$$

where  $\beta_t$  is a known parameter from the noise schedule [1] related to the  $t$ -th timestep,  $\nabla_{\mathbf{x}_t} \log p(\mathbf{x}_t)$  is the score function and  $\epsilon \sim \mathcal{N}(0, 1)$  is the Gaussian noise.

Then, by introducing the condition  $\mathbf{c}$ , Eq. 1 could be changed as:

$$\mathbf{x}_{t-1} = (1 + 0.5\beta_t)\mathbf{x}_t + \beta_t \nabla_{\mathbf{x}_t} \log p(\mathbf{x}_t | \mathbf{c}) + \sqrt{\beta_t}\epsilon, \quad (2)$$

where  $\mathbf{c}$  could be a reference image, a text, etc.

By using the Bayesian rule [6], we have:

$$\nabla_{\mathbf{x}_t} \log p(\mathbf{x}_t | \mathbf{c}) = \underbrace{\nabla_{\mathbf{x}_t} \log p(\mathbf{x}_t)}_{\text{Unconditional term}} + \underbrace{\nabla_{\mathbf{x}_t} \log p(\mathbf{c} | \mathbf{x}_t)}_{\text{Conditional term}}. \quad (3)$$

The target is to approximate the conditional term, which we also call guidance.

**Energy-based guidance.** Given an energy function  $\varepsilon(\mathbf{x}_t, \mathbf{c})$  as the metric to measure the distance between  $\mathbf{x}_t$  and  $\mathbf{c}$ , we have:

$$p(\mathbf{c} | \mathbf{x}_t) = \frac{\exp^{-\lambda\varepsilon(\mathbf{x}_t, \mathbf{c})}}{Z}. \quad (4)$$

where  $\lambda$  is a temperature coefficient and  $Z > 0$  is a normalizing constant.

Following the FreeDom [4], we could use the MMSE estimation  $\hat{\mathbf{x}}_{0|t}$  [6] of  $\mathbf{x}_t$  to measure the distance under the data domain instead of the noise domain since  $\hat{\mathbf{x}}_{0|t}$  could be regarded as the final results  $\mathbf{x}_0$  from  $t \rightarrow 0$  timestep. Therefore, the Eq. 4 could be defined as:

$$\log p(\mathbf{c} | \mathbf{x}_t) \approx \log p(\mathbf{c} | \hat{\mathbf{x}}_{0|t}) \propto \varepsilon(\hat{\mathbf{x}}_{0|t}, \mathbf{c}), \quad (5)$$

where

$$\begin{aligned} \hat{\mathbf{x}}_{0|t} &= \mathbb{E}(\mathbf{x}_0 | \mathbf{x}_t) \\ &\approx \frac{1}{\sqrt{\hat{\alpha}_t}}(\mathbf{x}_t + (1 - \hat{\alpha}_t)\epsilon_\theta(\mathbf{x}_t, t)), \end{aligned} \quad (6)$$

where  $\hat{\alpha}_t$  is also a known parameter from the noise schedule [1] related to the  $t$ -th timestep.

**Manifold preserving guided diffusion (MPGD).** Based on the linear manifold hypothesis [15], there is always a tangent space  $\mathcal{T}_{0|t}\mathcal{M}$  such that the  $\nabla_{\hat{\mathbf{x}}_{0|t}} p(\mathbf{c} | \hat{\mathbf{x}}_{0|t})$  lies on the tangent space. Then, we could define a new reverse process on  $\mathcal{T}_{0|t}\mathcal{M}$  as:

$$\begin{aligned} \mathbf{x}_{t-1} &= \mathbf{m}_t + \ell_t \epsilon_\theta(\mathbf{x}_t, t) + \sqrt{\beta_t}\epsilon, \\ \mathbf{m}_t &= \sqrt{\hat{\alpha}_{t-1}}(\hat{\mathbf{x}}_{0|t} - s_t \nabla_{\hat{\mathbf{x}}_{0|t}} \log p(\mathbf{c} | \hat{\mathbf{x}}_{0|t})), \end{aligned} \quad (7)$$

where  $s_t$  is a hyperparameter to control the strength of the guidance term and  $\ell_t$  is a known parameter calculated based on noise schedule.

**Challenge.** MPGD shown in Eq. 7 avoids calculating the partial part of the UNet to reduce the computation cost. Concretely, based on the Eq. 3-Eq. 4, we have:

$$\nabla_{\mathbf{x}_t} \log p(\mathbf{c}|\hat{\mathbf{x}}_{0|t}) = \frac{\partial \varepsilon(\hat{\mathbf{x}}_{0|t}, \mathbf{c})}{\partial \hat{\mathbf{x}}_{0|t}} \frac{\partial \hat{\mathbf{x}}_{0|t}}{\partial \mathbf{x}_t}. \quad (8)$$

For  $\frac{\partial \hat{\mathbf{x}}_{0|t}}{\partial \mathbf{x}_t}$ , we need to get the gradient of  $\varepsilon_\theta(*, *)$  and that is equal to get the gradients from the diffusion model. By implementing the Eq. 7, the  $\frac{\partial \hat{\mathbf{x}}_{0|t}}{\partial \mathbf{x}_t}$  part has been removed.

This remains a question that the performance of MPGD will be worse in other tasks compared with the performance in the inverse problem [15]. Based on the inverse problem, the condition  $\mathbf{c}$  is the result of the linear transform which lets the overall metric satisfy the linear assumption. This leads to MPGD being invalid in other tasks such as style guidance and face related guidance [4], which limits the generalization of MPGD.

Based on the information theory, we use the Fisher information to estimate the  $\frac{\partial \hat{\mathbf{x}}_{0|t}}{\partial \mathbf{x}_t}$  by leveraging the Cramér-Rao bound of Fisher information to replace  $\frac{\partial \hat{\mathbf{x}}_{0|t}}{\partial \mathbf{x}_t}$ , there is no additional assumption for our estimation. Thus it could be implemented in various downstream tasks since all the assumptions are satisfied by DMs. Then, we also offer a new insight into the behavior of  $\frac{\partial \hat{\mathbf{x}}_{0|t}}{\partial \mathbf{x}_t}$  and training-free methods.

## 4 Methodology

The main contribution of this paper is to introduce the Fisher information [20], which is an important metric to measure the reward of the information in a specific state. Then, we propose the Fisher information guided diffusion (FIGD) without any additional assumptions. In the end, we offer the theory analysis based on our theory to offer new insight.

**Fisher information guided diffusion.** We first expand  $\frac{\partial \hat{\mathbf{x}}_{0|t}}{\partial \mathbf{x}_t}$  by Eq. 6:

$$\begin{aligned} \frac{\partial \hat{\mathbf{x}}_{0|t}}{\partial \mathbf{x}_t} &= \frac{1}{\sqrt{\hat{\alpha}_t}} (1 + (1 - \hat{\alpha}_t) \frac{\partial \varepsilon_\theta(\mathbf{x}_t, t)}{\partial \mathbf{x}_t}) \\ &\propto \frac{\partial \varepsilon_\theta(\mathbf{x}_t, t)}{\partial \mathbf{x}_t}. \end{aligned} \quad (9)$$

Notice that  $\varepsilon_\theta(\mathbf{x}_t, t)$  is the approximation of the score function  $\nabla_{\mathbf{x}_t} \log p(\mathbf{x}_t)$ . The gradient of the score function is exactly the definition of the Fisher information [20]. Therefore, we define:

$$I(\mathbf{x}_t) = \frac{\partial \varepsilon_\theta(\mathbf{x}_t, t)}{\partial \mathbf{x}_t}, \quad (10)$$

where  $I(\mathbf{x}_t)$  is the Fisher information related to the variable  $\mathbf{x}_t$ .

Then, based on the central limited theorem [20],  $I(\mathbf{x}_t)$  will be convergent to the constant related to the time schedule:

**Theorem 1.** *Given the sequence  $\{\mathbf{x}_T, \mathbf{x}_{T-1}, \dots, \mathbf{x}_t, \dots, \mathbf{x}_1\}$ , where  $t \in [T, 0)$  and  $\mathbf{x}_T$  is the initial state of the reverse process, the  $I(\mathbf{x}_t)$  is convergent to the Cramér-Rao bound:*

$$\lim_{\Delta t \rightarrow 0} I(\mathbf{x}_{t+\Delta t}) = \frac{1}{1 - \hat{\alpha}_t}. \quad (11)$$

The detailed proofs and discussions are provided in the Appendix. A. Following the Theorem 1, we could get use the Cramér-Rao bound to estimate  $I(\mathbf{x}_t)$ :

**Theorem 2.** *For any  $\mathbf{x}_t$  where  $t \in [T, 0)$ , the Fisher information  $I(\mathbf{x}_t)$  could be bounded as:*

$$I(\mathbf{x}_t) < \lim_{\Delta t \rightarrow 0} I(\mathbf{x}_{t+\Delta t}) = \frac{1}{1 - \hat{\alpha}_t}. \quad (12)$$

---

**Algorithm 1** The overall algorithm for FIGD
 

---

**Input:**  $c, T, \epsilon_\theta$ , the noise schedule parameter  $\hat{\alpha}_t, \beta_t$ , the energy function  $\varepsilon$  and the hyperparameter  $\rho_t$ .  
**Output:**  $x_0$  ▷ The generated image based on  $c$

- 1:  $x_T \sim \mathcal{N}(0, 1)$
- 2: **for**  $t$  in  $[T - 1, \dots, 1]$  **do**
- 3:    $\epsilon \sim \mathcal{N}(0, 1)$
- 4:    $\mathbf{x}_{t-1} = (1 + 0.5\beta_t)\mathbf{x}_t + \beta_t \nabla_{\mathbf{x}_t} \log p(\mathbf{x}_t) + \sqrt{\beta_t} \epsilon$
- 5:    $\hat{\mathbf{x}}_{0|t} = \frac{1}{\sqrt{\hat{\alpha}_t}}(\mathbf{x}_t + (1 - \hat{\alpha}_t)\epsilon_\theta(\mathbf{x}_t, t))$  ▷ The MMSE method
- 6:    $g_t = \frac{2}{\sqrt{\hat{\alpha}_t}} \nabla_{\hat{\mathbf{x}}_{0|t}} \varepsilon(\hat{\mathbf{x}}_{0|t}, c)$
- 7:    $\mathbf{x}_{t-1} = \mathbf{x}_{t-1} - \rho_t g_t$
- 8: **end for**

**Return:**  $x_0$

---

The detailed proofs are provided in Appendix. A. We could replace the  $I(\mathbf{x}_t)$  by Cramér-Rao bound without any additional assumption. The Eq. 9 could be estimated as:

$$\frac{\partial \hat{\mathbf{x}}_{0|t}}{\partial \mathbf{x}_t} \approx \frac{2}{\sqrt{\hat{\alpha}_t}}. \quad (13)$$

By Eq. 8 and Eq. 13, we have:

$$\begin{aligned} \nabla_{\mathbf{x}_t} \log p(c|\hat{\mathbf{x}}_{0|t}) &\approx \frac{2}{\sqrt{\hat{\alpha}_t}} \frac{\partial \varepsilon(\hat{\mathbf{x}}_{0|t}, c)}{\partial \hat{\mathbf{x}}_{0|t}} \\ &= \frac{2}{\sqrt{\hat{\alpha}_t}} \nabla_{\hat{\mathbf{x}}_{0|t}} \log p(c|\hat{\mathbf{x}}_{0|t}). \end{aligned} \quad (14)$$

Then by Eq. 3 and Eq. 14, the sampling process of FIGD is:

$$\begin{aligned} \mathbf{x}_{t-1} &= \hat{\mathbf{m}}_{t-1} - \frac{2\rho_t}{\sqrt{\hat{\alpha}_t}} \nabla_{\hat{\mathbf{x}}_{0|t}} \varepsilon(\hat{\mathbf{x}}_{0|t}, c) \\ \hat{\mathbf{m}}_{t-1} &= (1 + 0.5\beta_t)\mathbf{x}_t + \beta_t \nabla_{\mathbf{x}_t} \log p(\mathbf{x}_t) + \sqrt{\beta_t} \epsilon, \end{aligned} \quad (15)$$

where  $\rho_t$  is the hyperparameter that is regarded as the learning rate to control the strength of guidance. The detailed algorithm is shown in Algorithm. 1

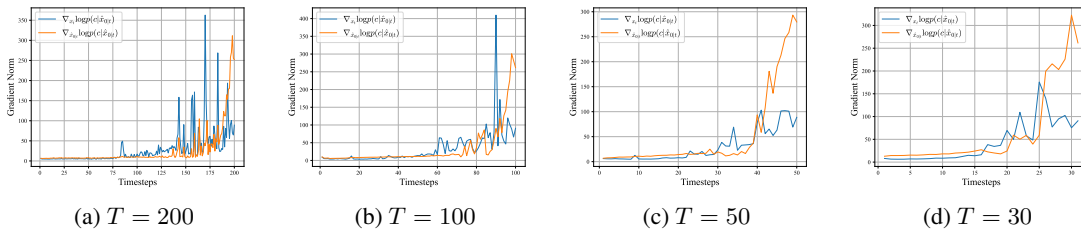


Figure 2: The comparison of the gradient norm based on the style guidance tasks with the stable diffusion. We show the value of the  $\|\nabla_{\mathbf{x}_t} \log p(c|\hat{\mathbf{x}}_{0|t})\|_2$  and  $\|\nabla_{\hat{\mathbf{x}}_{0|t}} \log p(c|\hat{\mathbf{x}}_{0|t})\|_2$  among different timesteps to show the influence via the Fisher information. Concretely (a), (b), (c), and (d) report the values under 200, 100, 50, and 30 sampling steps respectively.

**Theory analysis.** The other main contribution is using the Fisher information to interpret the gradient and training-free methods. To begin with,  $I(\mathbf{x}_t)$  measures the information that  $\mathbf{x}_t$  carried out in the  $t$ -th time.  $\nabla_{\mathbf{x}_t} \log p(c|\hat{\mathbf{x}}_{0|t})$  could be split into two parts: 1) the conditional gradient  $\frac{\partial \varepsilon(\hat{\mathbf{x}}_{0|t}, c)}{\partial \hat{\mathbf{x}}_{0|t}}$ , 2) The Fisher information term  $\frac{\partial \hat{\mathbf{x}}_{0|t}}{\partial \mathbf{x}_t}$ . Then, the Fisher information term decides how much information could be gained based on the direction of the conditional gradient. Thus, the overall term could be explained by how much information it could gain following the direction of the conditional gradient. For example, if the  $\|I(\mathbf{x}_t)\|_2$  is large,  $\mathbf{x}_{t-1}$  could get more information following the current conditional gradient in  $t$ -th time. If the  $\|I(\mathbf{x}_t)\|_2$  is small,  $\mathbf{x}_{t-1}$  will gain less information from the current conditional gradient and thus tends to be the unconditional state.

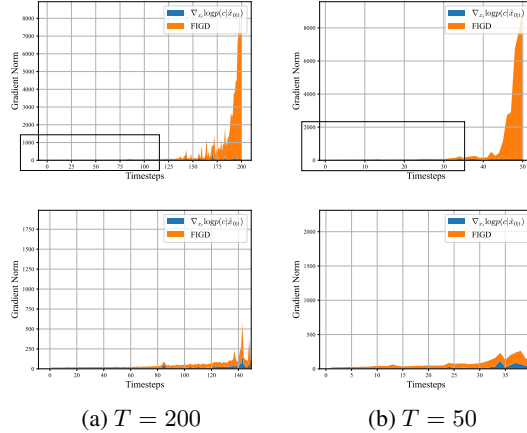


Figure 3: The comparison between FIGD and the FreeDom. (a) and (b) shows the value of the gradient norm between  $\nabla_{\mathbf{x}_t} \log p(\mathbf{c}|\hat{\mathbf{x}}_{0|t})$  and FIGD under  $T = 200$  and  $T = 50$  respectively.

We make the experiments based on the style guidance of the stable diffusion as an example to illustrate. As shown in Figure 2, the norm of the conditional gradient is decreasing when  $t$  tends to be 0 since  $\mathbf{x}_t$  is close enough to the  $\mathbf{c}$  when  $t \rightarrow 0$  and the gradient will not provide the information anymore. Influenced by the  $I(\mathbf{x}_t)$ , the norm of  $\nabla_{\mathbf{x}_t} \log p(\mathbf{c}|\hat{\mathbf{x}}_{0|t})$  has different trend compared with the norm of  $\nabla_{\hat{\mathbf{x}}_{0|t}} \log p(\mathbf{c}|\hat{\mathbf{x}}_{0|t})$ . Figure. 2(a) shows that the  $I(\mathbf{x}_t)$  is large during the middle state of the reverse process instead of decreasing from  $T \rightarrow 0$ . This demonstrates that the training-free methods highly depend on the middle phase of the reverse process since it can get more information. This also interprets the phenomenon found in FreeDom [4] that it is not necessary to implement guidance methods during the entire reverse process.

Then, we show why FIGD could work without any assumptions. In the early phase ( $t \in [T, 80\%T]$ ),  $I(\mathbf{x}_t)$  tends to be small which weakens the conditional gradient. The same trend shows in the latter phase ( $t \in [20\%T, 0)$ ). In this case, we have to make sure that there are enough steps for the middle phase of the reverse process. Meanwhile, with the decreasing number of sampling steps of the reverse process such as  $T = 30$  and  $T = 50$ , the  $\nabla_{\mathbf{x}_t} \log p(\mathbf{c}|\hat{\mathbf{x}}_{0|t})$  decrease dramatically as shown in Figure 2(c-d). This causes the guidance to lack enough information and thus leads the guidance to fail.

FIGD solves this problem by using the Cramér-Rao bound of the Fisher information to replace  $I(\mathbf{x}_t)$ . As shown in Figure. 3, we can find that during all stages, FIGD could get more information compared with calculating the entire partial. Under the few sampling steps ( $T = 50$ ), FIGD ensures that the guidance accumulates sufficient information in the direction of the conditional gradient. This is the main reason why FIGD could work even with a few sampling steps in some conditions such as style guidance tasks based on the stable diffusion since FIGD simply uses Cramér-Rao bound to increase the information gain during the entire reverse process, thus it does not require any assumptions.

## 5 Experiment

### 5.1 Experiment Settings

To show the ability of the FIGD, we focus on the tasks in which the differentiable metrics are nonlinear based on various open-source diffusion models. Similar to the FreeDom [4], the tasks, related models, and conditions we have tried are:

- **Face related tasks.** We use unconditional human face diffusion model [16] as the pre-trained model in these tasks. It supports generating human face related images with 256\*256 pre-trained from the CelebA-HQ [27]. We experiment with conditions including text, parsing maps, and sketches. We choose the DDIM sampler with  $T = 50$  for FIGD and  $T = 100$  for FreeDom and MPGD. Then, based on the different conditions, we define  $\varepsilon(\hat{\mathbf{x}}_{0|t}, \mathbf{c})$  as follows: 1) For text guidance, the  $\mathbf{c}$  is the text prompts. We use CLIP [28] to extract the vision embedding from  $\hat{\mathbf{x}}_{0|t}$  and text embedding from  $\mathbf{c}$ .  $\varepsilon(\hat{\mathbf{x}}_{0|t}, \mathbf{c})$  is the cosine similarity between embedding. 2) For parsing maps and sketches,  $\mathbf{c}$  are parsing maps and sketches respectively. We also use the CLIP to extract the vision embedding from both  $\hat{\mathbf{x}}_{0|t}$  and  $\mathbf{c}$ .  $\varepsilon(\hat{\mathbf{x}}_{0|t}, \mathbf{c})$  keeps the same definition with text guidance.

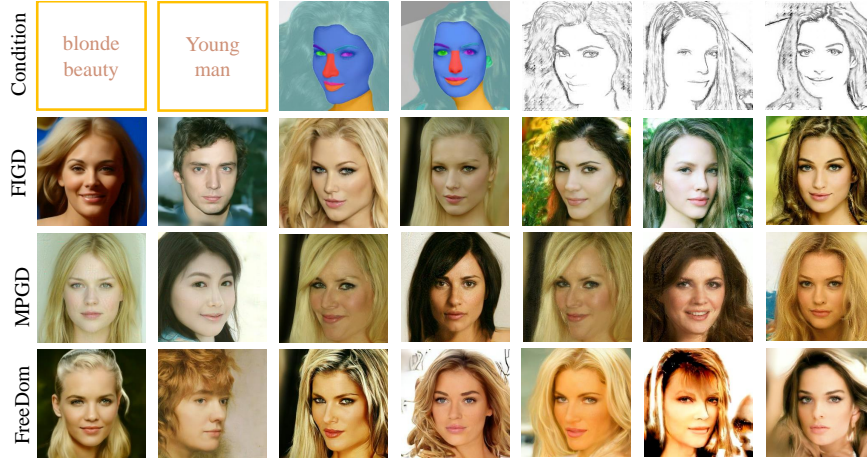


Figure 4: Qualitative examples of using a single condition human face images. The included conditions are: (a) text; (b) face parsing maps and (c) sketches. We compare the results with the MPGD and FreeDom. It can be found that MPGD is invalid since these tasks break the linear hypothesis theory and FIGD performs well.



Figure 5: Qualitative examples of style-guided generation with Stable Diffusion experiment based on FIGD compared with the FreeDom and the MPGD.

- **Style-guided generation with Stable Diffusion.** Stable diffusion is the text-to-image latent diffusion model with 512\*512 resolutions. We use the Stable diffusion V1.4 to experiment with the conditions of the style images. We chose the DDIM sampler with  $T = 100$  and  $T = 50$  for two baselines: MPGD and Freedom. We chose  $T = 50$  and  $T = 30$  for our method.  $c$  in this task are the style images. we use CLIP to calculate the norm of Gram matrix [4] as the  $\varepsilon(\hat{x}_{0|t}, c)$ .
- **ControlNet related generations with multiple guidance.** ControlNet [7] introduces various conditions such as depth maps and pose maps for stable diffusion. We experiment with the conditions, including FaceID and style images, to test our method in multi-conditions tasks.  $c$  here are the FaceID images and style images respectively. We both use the CLIP to extract the embedding and calculate the cosine similarity for FaceID and Gram matrix for style task as  $\varepsilon(\hat{x}_{0|t}, c)$  respectively.

Meanwhile, we use a single RTX4090 GPU to finish all the experiments. The baselines are two SOTA methods: *FreeDom* and *MPGD*. We use the time-travel strategy [4] and the default optimal hyperparameters for *FreeDom* and *MPGD* to make a fair comparison.

Method	Style↓	CLIP↑	Time(s)
LGD-MC ( $T = 100, MC = 1$ )	254.59	38.23	63
LGD-MC ( $T = 100, MC = 3$ )	247.39	39.39	NA
FreeDom ( $T = 100$ )	226.26	27.21	63
FreeDom ( $T = 50$ )	377.96	<b>32.54</b>	33
MPGD ( $T = 100$ )	351.16	25.08	35
MPGD ( $T = 50$ )	408.28	23.23	18
FIGD ( $T = 100$ )	<b>225.83</b>	<b>52.39</b>	<b>27</b>
FIGD ( $T = 50$ )	<b>245.51</b>	30.84	<b>17</b>
FIGD ( $T = 30$ )	<b>281.67</b>	29.07	<b>11</b>

Table 1: Quantitative results of style-guided generation with Stable Diffusion experiment. We compared FIGD with the two baselines, FreeDom and MPGD, in style-guided generation tasks with the Stable Diffusion; we get the overall improvement both in the Style score [4], CLIP score and the time cost since our method could generate high-quality images with few sampling steps.

Method	Pose Distance↓	Time(s)
FreeDom	54.21	193
FIGD	<b>40.01</b>	<b>130</b>

Table 2: Qualitative results of face related tasks based on ControlNet experiments, where Pose distance is the distance norm between pose maps and generated images.

## 5.2 Qualitative Results

**Face related tasks.** To begin with, we first show the result of FIGD in face-related tasks including text, face parsing maps, and sketches shown in Figure 4. It could be found that FIGD generates high-quality images related to the condition compared with the MPGD. Meanwhile, compared with the FreeDom, FIGD generates similar images. This proves the validity of our theory analysis that in the conditional generation except for the inverse problems, the strong assumption of MPGD will lead to fail generation and FIGD overcomes this problem.

**Style-guided generation with Stable Diffusion.** To further show the potential of the FIGD, we change the tasks to the style transfer based on the diffusion model shown in Figure 5. This task is more complicated compared with the face-related tasks since there are two guidance: 1) the text prompts and 2) the style image. It could be found that FIGD achieves high-quality generations within the same sampling steps compared with the MPGD. Then, to support the effectiveness of the FIGD, we make a comparison with the FreeDom. Our method still generated better cats. We also make the quantitative results of style-guided generation shown in Table 1, where FIGD achieves the best balance between style score and CLIP scores.

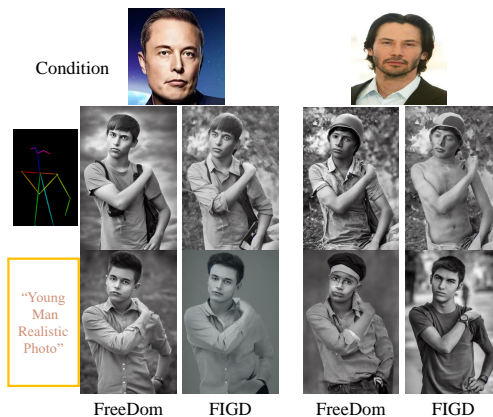


Figure 6: Qualitative examples of face related tasks based on ControlNet experiments. We compared FIGD with the FreeDom.



Figure 7: Qualitative examples of the style task based on ControlNet experiments. We compared FIGD with the FreeDom. The text prompts are "bike" for sketch bike and "ice-cream cone" for sketch ice-cream cone respectively.

Method	CLIP $\uparrow$	Style $\downarrow$	Time(s)
FreeDom	66.67	282.25	299
FIGD	53.18	244.5	32

Table 3: Qualitative results of style image guidance with ControlNet experiments, where CLIP is the cosine similarity of the clip embedding of generated images and sketch, Style is the distance norm between style images and generated images.

**ControlNet related generations with multiple guidance.** To further show the effectiveness of the FIGD, following the FreeDom, we implement it in the multiple guidance tasks based on the ControlNet. There are two tasks and the first task is the *face guidance* task shown in Figure 6, where we use the text prompts and pose mappings as the input of ControlNet to generate the images with similar poses and satisfy the description of text prompts. In this condition, we add face ID images as the independent condition to guide the ControlNet to generate similar faces and poses that satisfy the text prompt and face ID. The other task is the *style task*, where we change the condition of the ControlNet to the sketch and use the style image as the independent guidance to prove the feasibility of the FIGD shown in Figure 7. Since the performance of the MPGD is below that of the FreeDom, we do not make a comparison in these challenge tasks.

**Abation study for  $\rho_t$ .** We study the effect of  $\rho_t$  from small to large shown ( $\rho_t = 1$  as the beginning) in Figure 8. We can see that FIGD is scalable and the user can set different values according to the requirements.

## 6 Conclusion

We proposed the Fisher information guided diffusion to achieve the condition generation. Concretely, we introduce the Fisher information to estimate the gradient of the conditional term by leveraging the Cramér-Rao bound based on the central limited theorem. In this way, we could avoid calculating the gradient of the UNet while keeping high generation quality without any additional assumptions. In part of the tasks such as style image condition based on stable diffusion, we even reduce half of the sampling timestep. In the end, based on the information theory, we analyze the reason why FIGD could work and offer a new view for training-free methods.

**Limitation.** However, our method still has limitations. Firstly our theory reveals that there is conflict that could be caused by multi-conditions and out-of-distribution problems. They will lead the Fisher information to be huge fluctuation if the multi conditions are not dependent and if the pre-trained diffusion model is trained in a small dataset such as CelebA-HQ. The multi-conditions problem is obvious in the ControlNet. For example, we give a prompt: "a bike" and give a sketch drawn with the dog as the condition. This will lead to a low-quality generation. Meanwhile,



Figure 8: Demonstration of the effect of different  $\rho_t$  from small scale to large scale based on the style transfer task of stable diffusion. The top images are style images. The text prompt is: "a cat wearing glasses".

FIGD will increase the information for the guidance which leads to the generated image ignoring the other conditions from the ControlNet. In this condition, we need to choose a suitable  $\rho_t$  and design a better metric. In future work, we will further study how to solve these problems and let our method be more generalization.

## Impact Statements

This paper presents work whose goal is to advance the field of Deep Learning. There are many potential societal consequences of our work, none which we feel must be specifically highlighted here.

## References

- [1] Jonathan Ho, Ajay Jain, and Pieter Abbeel. Denoising diffusion probabilistic models. *CoRR*, abs/2006.11239, 2020.
- [2] Ian J. Goodfellow, Jean Pouget-Abadie, Mehdi Mirza, Bing Xu, David Warde-Farley, Sherjil Ozair, Aaron Courville, and Yoshua Bengio. Generative adversarial networks, 2014.
- [3] Jaeseok Jeong, Mingi Kwon, and Youngjung Uh. Training-free content injection using h-space in diffusion models, 2024.
- [4] Jiwen Yu, Yinhuai Wang, Chen Zhao, Bernard Ghanem, and Jian Zhang. Freedom: Training-free energy-guided conditional diffusion model. *Proceedings of the IEEE/CVF International Conference on Computer Vision (ICCV)*, 2023.
- [5] Junjiao Tian, Lavisha Aggarwal, Andrea Colaco, Zsolt Kira, and Mar González-Franco. Diffuse, attend, and segment: Unsupervised zero-shot segmentation using stable diffusion. *CoRR*, abs/2308.12469, 2023.
- [6] Hyungjin Chung, Jeongsol Kim, Michael Thompson Mccann, Marc Louis Klasky, and Jong Chul Ye. Diffusion posterior sampling for general noisy inverse problems. In *The Eleventh International Conference on Learning Representations*, 2023.
- [7] Lymin Zhang, Anyi Rao, and Maneesh Agrawala. Adding conditional control to text-to-image diffusion models, 2023.
- [8] Ramprasaath R. Selvaraju, Michael Cogswell, Abhishek Das, Ramakrishna Vedantam, Devi Parikh, and Dhruv Batra. Grad-cam: Visual explanations from deep networks via gradient-based localization. *International Journal of Computer Vision*, 128(2):336–359, October 2019.
- [9] Robin Rombach, Andreas Blattmann, Dominik Lorenz, Patrick Esser, and Björn Ommer. High-resolution image synthesis with latent diffusion models, 2021.
- [10] Alex Nichol, Prafulla Dhariwal, Aditya Ramesh, Pranav Shyam, Pamela Mishkin, Bob McGrew, Ilya Sutskever, and Mark Chen. Glide: Towards photorealistic image generation and editing with text-guided diffusion models, 2022.
- [11] Bram Wallace, Akash Gokul, Stefano Ermon, and Nikhil Naik. End-to-end diffusion latent optimization improves classifier guidance, 2023.

- [12] Chenlin Meng, Yutong He, Yang Song, Jiaming Song, Jiajun Wu, Jun-Yan Zhu, and Stefano Ermon. Sdedit: Guided image synthesis and editing with stochastic differential equations, 2022.
- [13] Narek Tumanyan, Michal Geyer, Shai Bagon, and Tali Dekel. Plug-and-play diffusion features for text-driven image-to-image translation. In *Proceedings of the IEEE/CVF Conference on Computer Vision and Pattern Recognition (CVPR)*, pages 1921–1930, June 2023.
- [14] Jiaming Song, Arash Vahdat, Morteza Mardani, and Jan Kautz. Pseudoinverse-guided diffusion models for inverse problems. In *The Eleventh International Conference on Learning Representations, ICLR 2023, Kigali, Rwanda, May 1-5, 2023*, 2023.
- [15] Yutong He, Naoki Murata, Chieh-Hsin Lai, Yuhta Takida, Toshimitsu Uesaka, Dongjun Kim, Wei-Hsiang Liao, Yuki Mitsufuji, J. Zico Kolter, Ruslan Salakhutdinov, and Stefano Ermon. Manifold preserving guided diffusion, 2023.
- [16] Yang Song, Jascha Sohl-Dickstein, Diederik P Kingma, Abhishek Kumar, Stefano Ermon, and Ben Poole. Score-based generative modeling through stochastic differential equations. In *International Conference on Learning Representations*, 2021.
- [17] Jiaming Song, Chenlin Meng, and Stefano Ermon. Denoising diffusion implicit models, 2022.
- [18] Hyungjin Chung, Byeongsu Sim, Dohoon Ryu, and Jong Chul Ye. Improving diffusion models for inverse problems using manifold constraints, 2022.
- [19] Bowen Song, Soo Min Kwon, Zecheng Zhang, Xinyu Hu, Qing Qu, and Liyue Shen. Solving inverse problems with latent diffusion models via hard data consistency, 2023.
- [20] Andrew R. Barron. Entropy and the central limit theorem. *The Annals of Probability*, 14(1):336–342, 1986.
- [21] Nataniel Ruiz, Yuanzhen Li, Varun Jampani, Yael Pritch, Michael Rubinstein, and Kfir Aberman. Dreambooth: Fine tuning text-to-image diffusion models for subject-driven generation. In *IEEE/CVF Conference on Computer Vision and Pattern Recognition, CVPR 2023, Vancouver, BC, Canada, June 17-24, 2023*, pages 22500–22510, 2023.
- [22] Chen Henry Wu and Fernando De la Torre. A latent space of stochastic diffusion models for zero-shot image editing and guidance. In *ICCV*, 2023.
- [23] Zalan Fabian, Berk Tinaz, and Mahdi Soltanolkotabi. Adapt and diffuse: Sample-adaptive reconstruction via latent diffusion models, 2023.
- [24] Xianghao Kong, Rob Brekelmans, and Greg Ver Steeg. Information-theoretic diffusion. In *International Conference on Learning Representations*, 2023.
- [25] Yingheng Wang, Yair Schiff, Aaron Gokaslan, Weishen Pan, Fei Wang, Christopher De Sa, and Volodymyr Kuleshov. InfoDiffusion: Representation learning using information maximizing diffusion models. In *Proceedings of the 40th International Conference on Machine Learning*, pages 36336–36354, 2023.
- [26] Xianghao Kong, Ollie Liu, Han Li, Dani Yogatama, and Greg Ver Steeg. Interpretable diffusion via information decomposition, 2023.
- [27] Tero Karras, Timo Aila, Samuli Laine, and Jaakko Lehtinen. Progressive growing of gans for improved quality, stability, and variation. In *6th International Conference on Learning Representations, ICLR 2018, Vancouver, BC, Canada, April 30 - May 3, 2018, Conference Track Proceedings*, 2018.
- [28] Alec Radford, Jong Wook Kim, Chris Hallacy, Aditya Ramesh, Gabriel Goh, Sandhini Agarwal, Girish Sastry, Amanda Askell, Pamela Mishkin, Jack Clark, Gretchen Krueger, and Ilya Sutskever. Learning transferable visual models from natural language supervision, 2021.

## 7 Appendix

### 8 PROOFS AND THEORETICAL ANALYSIS

#### 8.1 PROOF OF THEOREM 1

**Theorem 8.1.** Given the sequence  $\{\mathbf{x}_T, \mathbf{x}_{T-1}, \dots, \mathbf{x}_t, \dots, \mathbf{x}_1\}$ , where  $t \in [T, 0)$  and  $\mathbf{x}_T$  is the initial state of the reverse process, the  $I(\mathbf{x}_t)$  is convergent to the Cramér-Rao bound:

$$\lim_{\Delta t \rightarrow 0} I(\mathbf{x}_{t+\Delta t}) = \frac{1}{1 - \hat{\alpha}_t}. \quad (8.1)$$

*Proof.* The reverse process of the diffusion model could be formulated as:

$$\mathbf{x}_{t-1} = \sqrt{\alpha_{t-1}} \left( \frac{\mathbf{x}_t - \sqrt{1 - \alpha_t} \epsilon_\theta(\mathbf{x}_t, t)}{\sqrt{\alpha_t}} \right) + \sqrt{1 - \alpha_{t-1} - \sigma_t^2} \epsilon_\theta(\mathbf{x}_t, t) + \sigma_t \epsilon, \quad (8.2)$$

where  $\alpha_{t-1}$ ,  $\alpha_t$ ,  $\sigma_t$  are the known parameters related to the noise schedule,  $\epsilon_\theta \sim \mathcal{N}(0, 1)$  is the pure Gaussian noise and  $\epsilon_\theta(*, *)$  are the score function based on the parameter  $\theta$ .

Then we organize Eq. 8.2 as:

$$\mathbf{x}_{t-1} = \frac{\sqrt{\alpha_{t-1}}}{\sqrt{\alpha_t}} \mathbf{x}_t + \mathbf{m}_t \epsilon_\theta(\mathbf{x}_t, t) + \sigma_t \epsilon. \quad (8.3)$$

where:

$$\mathbf{m}_t = \sqrt{1 - \alpha_{t-1} - \sigma_t^2} - \frac{\sqrt{\alpha_{t-1}}}{\sqrt{\alpha_t}} (\sqrt{1 - \alpha_t}). \quad (8.4)$$

We could build the time sequence related to the  $\mathbf{x}_t$  based on Eq. 8.3 during  $[t + \Delta t, t]$  as  $S_n = \{\mathbf{x}_{t+\Delta t}, \dots, \mathbf{x}_t\}$ , where  $n$  is sampling iterations. Then, recall the forward process:

$$\mathbf{x}_t = \frac{\sqrt{\alpha_t}}{\sqrt{\alpha_{t-1}}} \mathbf{x}_{t-1} + \left(1 - \frac{\alpha_t}{\alpha_{t-1}}\right) \epsilon. \quad (8.5)$$

Based on the property of the diffusion model, given the well pre-trained  $\epsilon_\theta(\mathbf{x}_t, t)$ , we have:

$$\mathbf{m}_t \epsilon_\theta(\mathbf{x}_t, t) + \sigma_t \epsilon \approx \left(1 - \frac{\alpha_t}{\alpha_{t-1}}\right) \epsilon. \quad (8.6)$$

By  $j_t = \frac{\alpha_t}{\alpha_{t-1}}$ , we further have:

$$\mathbf{x}_{t-1} = \sqrt{j_t} \mathbf{x}_t + \sqrt{1 - j_t} \epsilon. \quad (8.7)$$

In this way, the samples in  $S_n$  satisfies the central limit theorem [20]:

$$\lim_{\Delta t \rightarrow 0} I(\mathbf{x}_{t+\Delta t}) = \frac{1}{1 - \hat{\alpha}_t}. \quad (8.8)$$

Thus, we finish the proof.  $\square$

#### 8.2 PROOF OF THEOREM 8.2

**Theorem 8.2.** For any  $\mathbf{x}_t$  where  $t \in [T, 0)$ , the Fisher information  $I(\mathbf{x}_t)$  could be bounded as:

$$I(\mathbf{x}_t) < \lim_{\Delta t \rightarrow 0} I(\mathbf{x}_{t+\Delta t}) = \frac{1}{1 - \hat{\alpha}_t}. \quad (8.9)$$

*Proof.* Based on the Theorem 1 and Eq. 8.7, given the continuous time sequence  $S_n$ , for any time we all have the Cramér-Rao bound. Based on the property of the stochastic differential equation [16], during  $[t + \Delta t, t]$ , we could build the time sequence  $S_n$  in each  $t$ . Therefore, in each  $t$ , it always exists the Cramér-Rao bound and thus we could use the Cramér-Rao bound as the estimate of  $I(\mathbf{x}_t)$ . Then, with the decreasing of  $t$ ,  $\hat{\alpha}_t$  will decrease. For  $t + \Delta t > t$ , we all have  $I(\mathbf{x}_t) < \lim_{\Delta t \rightarrow 0} I(\mathbf{x}_{t+\Delta t})$ . Thus, we finish the proof.  $\square$

### 8.3 ESTIMATION ERROR

In this section, we analyze the estimation error of FIGD with the MPGD.

**Proposition 1.** *Given a precise energy function  $\varepsilon(\hat{\mathbf{x}}_{0|t}, \mathbf{c})$ , the reverse process of the FIGD could be formulated as:*

$$\begin{aligned}\mathbf{x}_{t-1} &= \hat{m}_{t-1} - \frac{2\rho_t}{\sqrt{\hat{a}_t}} \nabla_{\hat{\mathbf{x}}_{0|t}} \varepsilon(\hat{\mathbf{x}}_{0|t}, \mathbf{c}) \\ \hat{m}_{t-1} &= (1 + 0.5\beta_t)\mathbf{x}_t + \beta_t \nabla_{\mathbf{x}_t} \log p(\mathbf{x}_t) + \sqrt{\beta_t} \epsilon.\end{aligned}\tag{8.10}$$

Assumes  $\varepsilon(\hat{\mathbf{x}}_{0|t}, \mathbf{c})$  following  $\kappa$ -Lipschitz, we have the upper bound:

$$\|x_t^{FIGD} - x_t^{MPGD}\|_2 < \rho_t \kappa \left( \frac{2\sqrt{\hat{a}_{t-1}} - \sqrt{\hat{a}_t}}{\sqrt{\hat{a}_t}} \right).\tag{8.11}$$

*Proof.* Based on the  $\kappa$ -Lipschitz, we first have:

$$\nabla_{\hat{\mathbf{x}}_{0|t}} \varepsilon(\hat{\mathbf{x}}_{0|t}, \mathbf{c}) < \kappa.\tag{8.12}$$

Then:

$$\begin{aligned}\|x_t^{FIGD} - x_t^{MPGD}\|_2 &= \rho_t \left\| \frac{2}{\sqrt{\hat{a}_t}} \nabla_{\hat{\mathbf{x}}_{0|t}} \varepsilon(\hat{\mathbf{x}}_{0|t}, \mathbf{c}) - \sqrt{\hat{a}_{t-1}} \nabla_{\hat{\mathbf{x}}_{0|t}} \varepsilon(\hat{\mathbf{x}}_{0|t}, \mathbf{c}) \right\|_2 \\ &\approx \rho_t \left( \frac{2\sqrt{\hat{a}_{t-1}} - \sqrt{\hat{a}_t}}{\sqrt{\hat{a}_t}} \right) \|\nabla_{\hat{\mathbf{x}}_{0|t}} \varepsilon(\hat{\mathbf{x}}_{0|t}, \mathbf{c})\|_2 \\ &< \rho_t \kappa \left( \frac{2\sqrt{\hat{a}_{t-1}} - \sqrt{\hat{a}_t}}{\sqrt{\hat{a}_t}} \right)\end{aligned}\tag{8.13}$$

Thus, we finish the proof. When  $t \rightarrow T$ ,  $\frac{2\sqrt{\hat{a}_{t-1}} - \sqrt{\hat{a}_t}}{\sqrt{\hat{a}_t}}$  will tend to be large. This further shows the difference between FIGD and MPGD. Meanwhile, when  $t \rightarrow 0$ ,  $\frac{2\sqrt{\hat{a}_{t-1}} - \sqrt{\hat{a}_t}}{\sqrt{\hat{a}_t}}$  will tend to 0.  $\square$

## 9 MORE RESULTS

### 9.1 FACE RELATED TASKS

**Text.** Given a pre-trained CLIP, we define that  $\mathcal{P}_{\theta_1}$  is the vision encoder and  $\mathcal{P}_{\theta_2}$  is the text encoder, the loss function could be defined as:

$$\varepsilon(\hat{\mathbf{x}}_{0|t}, \mathbf{c}) = \|\mathcal{P}_{\theta_1}(\hat{\mathbf{x}}_{0|t}) - \mathcal{P}_{\theta_2}(\mathbf{c})\|_2,\tag{9.14}$$

where in this task,  $\mathbf{c}$  is the set of text prompts.

**Parse maps.** Given a pre-trained parse map extractor  $\mathcal{P}_{\theta_3}$  that could map the map to the parse map, the loss function could be defined as:

$$\varepsilon(\hat{\mathbf{x}}_{0|t}, \mathbf{c}) = \|\mathcal{P}_{\theta_3}(\hat{\mathbf{x}}_{0|t}) - \mathcal{P}_{\theta_3}(\mathbf{c})\|_2,\tag{9.15}$$

where in this task,  $\mathbf{c}$  is the set of reference images.

**Sketch.** Given a pre-trained sketch extractor  $\mathcal{P}_{\theta_4}$  that could change the image to the related sketch, the loss function could be defined as:

$$\varepsilon(\hat{\mathbf{x}}_{0|t}, \mathbf{c}) = \|\mathcal{P}_{\theta_4}(\hat{\mathbf{x}}_{0|t}) - \mathcal{P}_{\theta_4}(\mathbf{c})\|_2,\tag{9.16}$$

where in this task,  $\mathbf{c}$  is the set of reference images.

### 9.2 STABLE DIFFUSION RELATED TASKS

Given a pre-trained CLIP with the vision encoder  $\mathcal{P}_{\theta_1}$ , the loss function could be defined as:

$$\varepsilon(\hat{\mathbf{x}}_{0|t}, \mathbf{c}) = \|G(\mathcal{P}_{\theta_1}(\hat{\mathbf{x}}_{0|t})) - G(\mathcal{P}_{\theta_1}(\mathbf{c}))\|_2,\tag{9.17}$$

where  $G(*)$  is the operation to calculate the Gram matrix and  $\mathbf{c}$  is the set of style reference images.

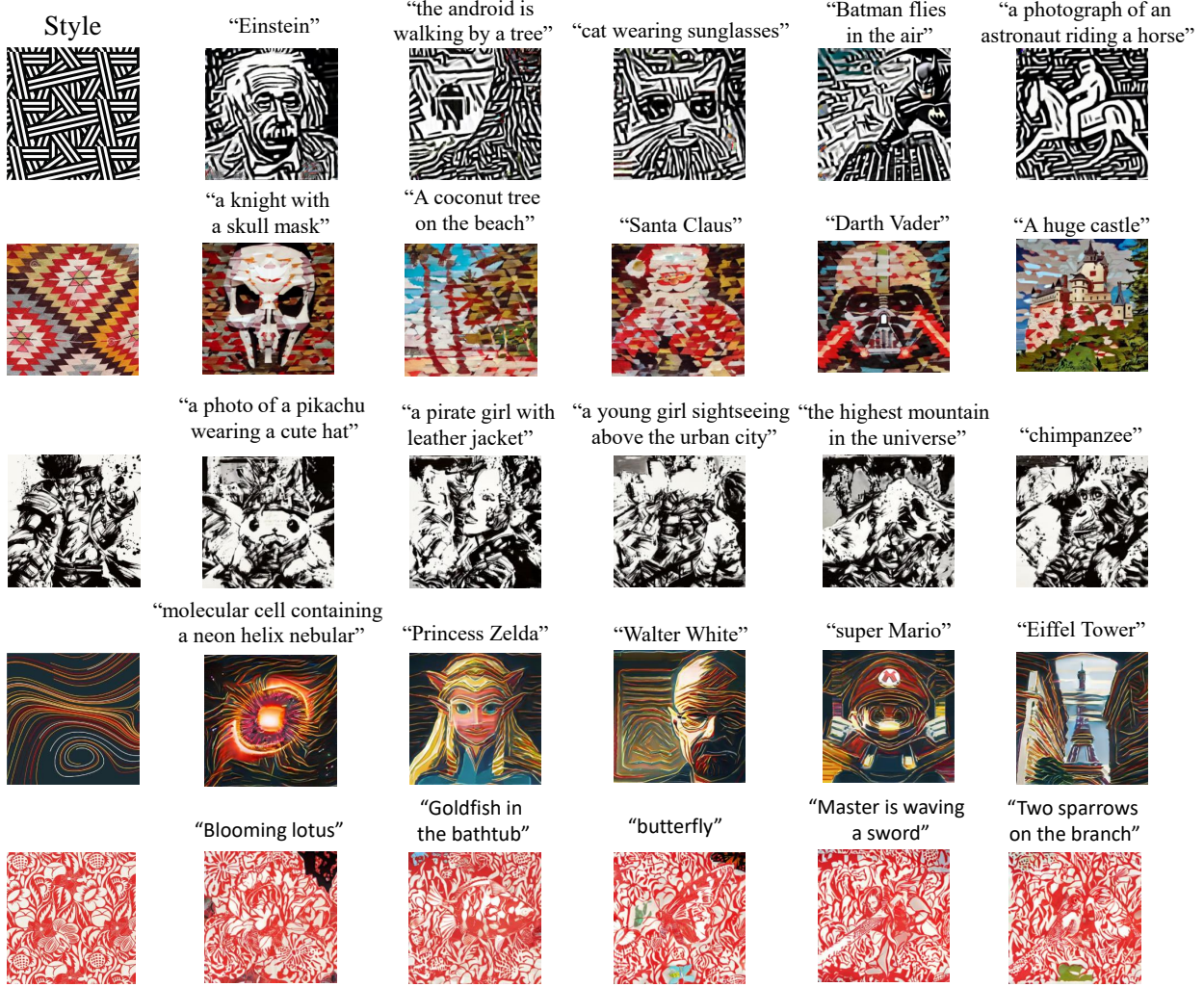


Figure 9: Generation results of training-free style guidance with text-to-image Stable Diffusion. We choose the five styles with different text prompts. It could be found that the generated images well match text prompts and style images.

### 9.3 CONTROLNET RELATED TASKS

**Face guidance.** Given a pre-trained face detector  $\mathcal{P}_{\theta_5}$  that could extract the face location with a bounding Box (bbox) and pre-trained parse map extractor  $\mathcal{P}_{\theta_3}$ , we first extract the bbox of the face and use the  $\mathcal{P}_{\theta_3}$  to extract related parse map as the guidance. The loss function could be defined as:

$$\varepsilon(\hat{\mathbf{x}}_{0|t}, \mathbf{c}) = \|\mathcal{P}_{\theta_5}(\mathcal{P}_{\theta_3}(\hat{\mathbf{x}}_{0|t})) - \mathcal{P}_{\theta_5}(\mathcal{P}_{\theta_3}(\mathbf{c}))\|_2, \quad (9.18)$$

where  $\mathbf{c}$  is the set of face reference images.

**Style task.** The loss function is the same as the loss function in stable diffusion-related tasks. Given a pre-trained CLIP with the vision encoder  $\mathcal{P}_{\theta_1}$ , the loss function could be defined as:

$$\varepsilon(\hat{\mathbf{x}}_{0|t}, \mathbf{c}) = \|G(\mathcal{P}_{\theta_1}(\hat{\mathbf{x}}_{0|t})) - G(\mathcal{P}_{\theta_1}(\mathbf{c}))\|_2. \quad (9.19)$$

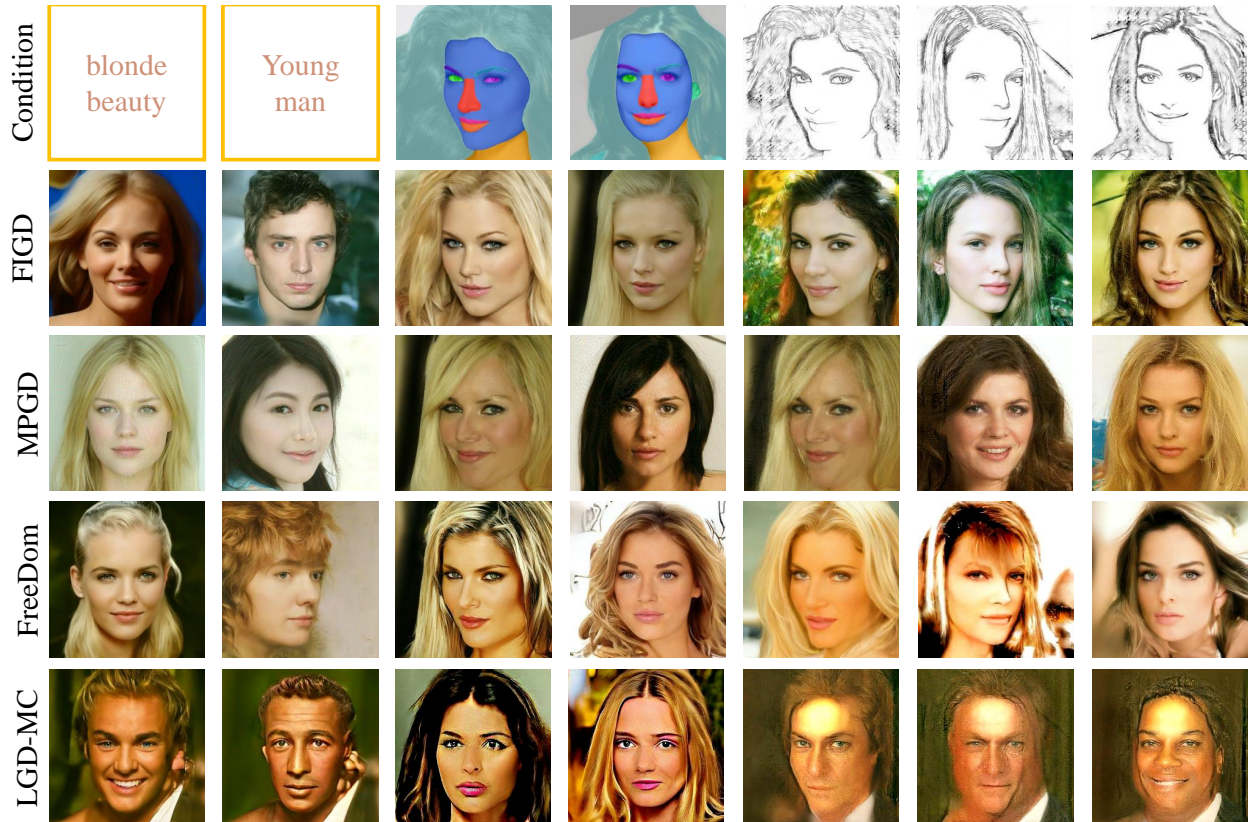


Figure 10: Qualitative examples of using a single condition human face images. The included conditions are (a) text, (b) face parsing maps, and (c) sketches. We compare FIGD ( $T = 50$ ) with the MPGD ( $T = 100$ ), FreeDom ( $T = 100$ ), and LGD-MC ( $T = 100, n = 3$ ). It can be found that MPGD is invalid since these tasks break the linear hypothesis theory, and FIGD performs well.

Table 4: Quantitative results of face-related tasks. We compare three FreeDom, LGD-MC, and MPGD based on CLIP score for text tasks and FID and distance norms for sketch and parse tasks.

Method	Texts	Parsing maps		Sketch	
	Distance↓	FID↓	Distance↓	FID↓	Distance↓
LGD-MC (T=100, n=3)	12.90	125.50	3225.13	144.74	43.40
FreeDom (T=100)	10.56	<b>117.77</b>	<b>2157.22</b>	146.43	39.94
MPGD (T=100)	12.26	175.31	2837.81	154.83	28.69
FIGD (T=100)	<b>10.16</b>	127.48	2224.98	<b>138.80</b>	<b>27.95</b>

## 10 MORE QUALITATIVE RESULTS

### 10.1 FACE RELATED TASKS

### 10.2 STABLE DIFFUSION RELATED TASKS

### 10.3 CONTROLNET RELATED TASKS

### 10.4 Extra Results



Figure 11: Quantitative results of training-free style guidance with text-to-image Stable Diffusion.

Table 5: Quantitative results of style-guided generation with Stable Diffusion experiment. We compared FIGD with the two baselines, FreeDom and MPGD, in style-guided generation tasks with the Stable Diffusion; we get the overall improvement both in the Style score [4], CLIP score and the time cost since our method could generate high-quality images with few sampling steps. NA for LGD-MC ( $T = 100, n = 3$ ) represents that we use shared memory to generate images since the required GPU RAM is over 24GB, and we cannot calculate the precise GPU costs.

Method	Style↓	CLIP↑	Time(s)
LGD-MC ( $T = 100, n = 1$ )	254.59	30.99	63
LGD-MC ( $T = 100, n = 3$ )	247.39	31.28	NA
FreeDom ( $T = 100$ )	226.26	27.21	63
FreeDom ( $T = 50$ )	377.96	<b>32.54</b>	33
MPGD ( $T = 100$ )	351.16	25.08	35
MPGD ( $T = 50$ )	408.28	23.23	18
FIGD ( $T = 100$ )	<b>225.83</b>	31.87	35
FIGD ( $T = 50$ )	245.51	30.84	17
FIGD ( $T = 30$ )	281.67	29.07	<b>11</b>



Figure 12: Additional quantitative results of training-free style guidance with text-to-image Stable Diffusion, where we use  $T = 100$  for FreeDom, MPGD and LGD-MC ( $n=3$ ) and use  $T = 50$  for FIGD.

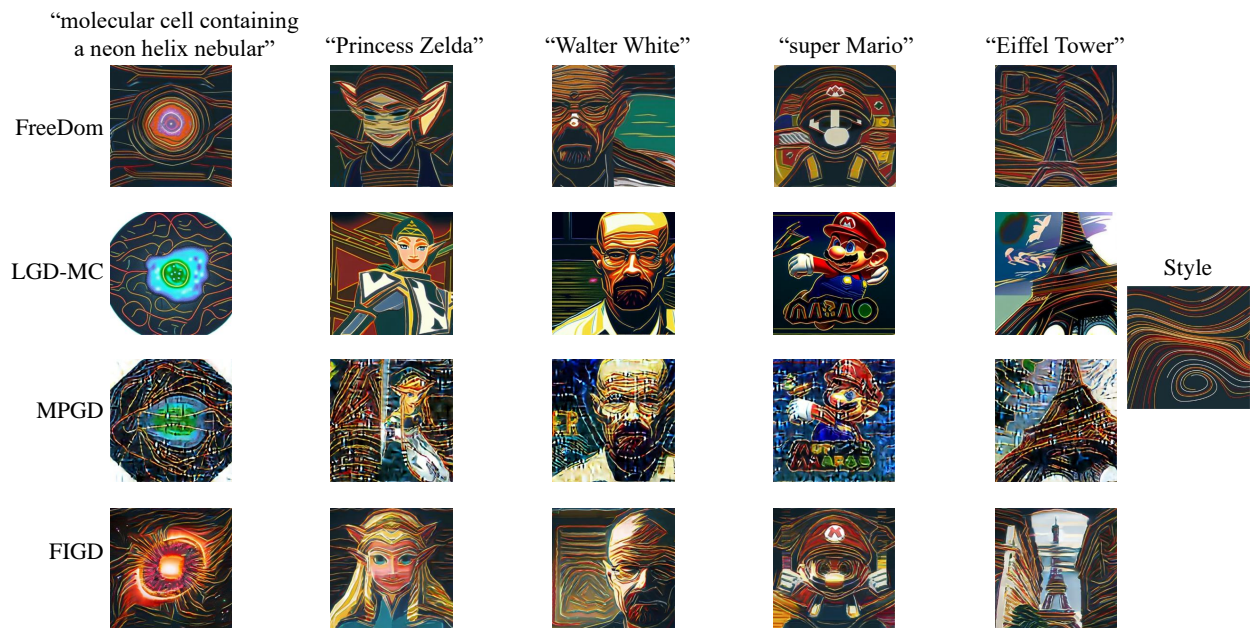


Figure 13: Additional quantitative results of training-free style guidance with text-to-image Stable Diffusion, where we use  $T = 100$  for FreeDom, MPGD and LGD-MC ( $n=3$ ) and use  $T = 50$  for FIGD.

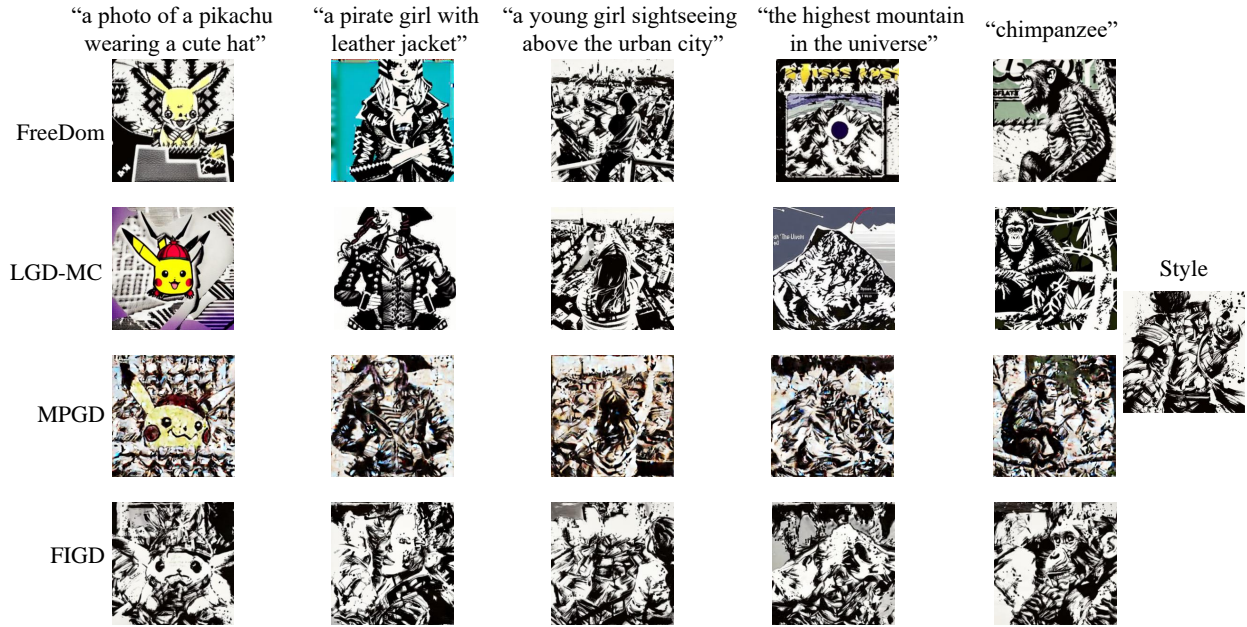


Figure 14: Additional quantitative results of training-free style guidance with text-to-image Stable Diffusion, where we use  $T = 100$  for FreeDom, MPGD and LGD-MC ( $n=3$ ) and use  $T = 50$  for FIGD.



Figure 15: Additional quantitative results of training-free style guidance with text-to-image Stable Diffusion, where we use  $T = 100$  for FreeDom, MPGD and LGD-MC ( $n=3$ ) and use  $T = 50$  for FIGD.

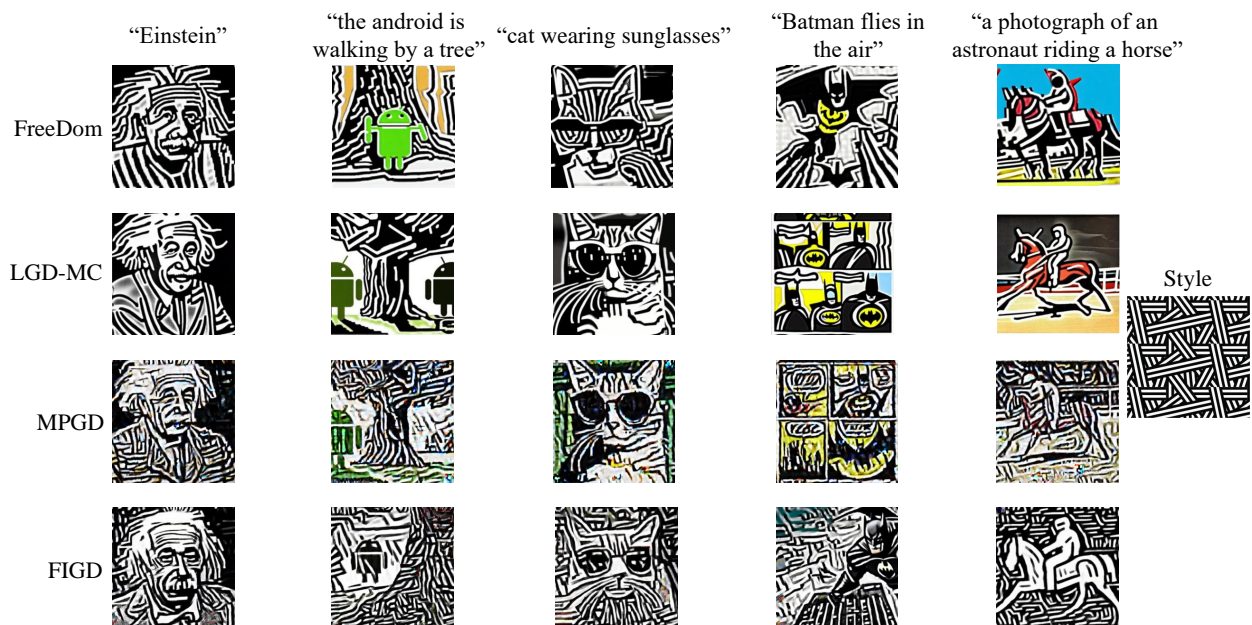


Figure 16: Additional quantitative results of training-free style guidance with text-to-image Stable Diffusion, where we use  $T = 100$  for FreeDom, MPGD and LGD-MC ( $n=3$ ) and use  $T = 50$  for FIGD.

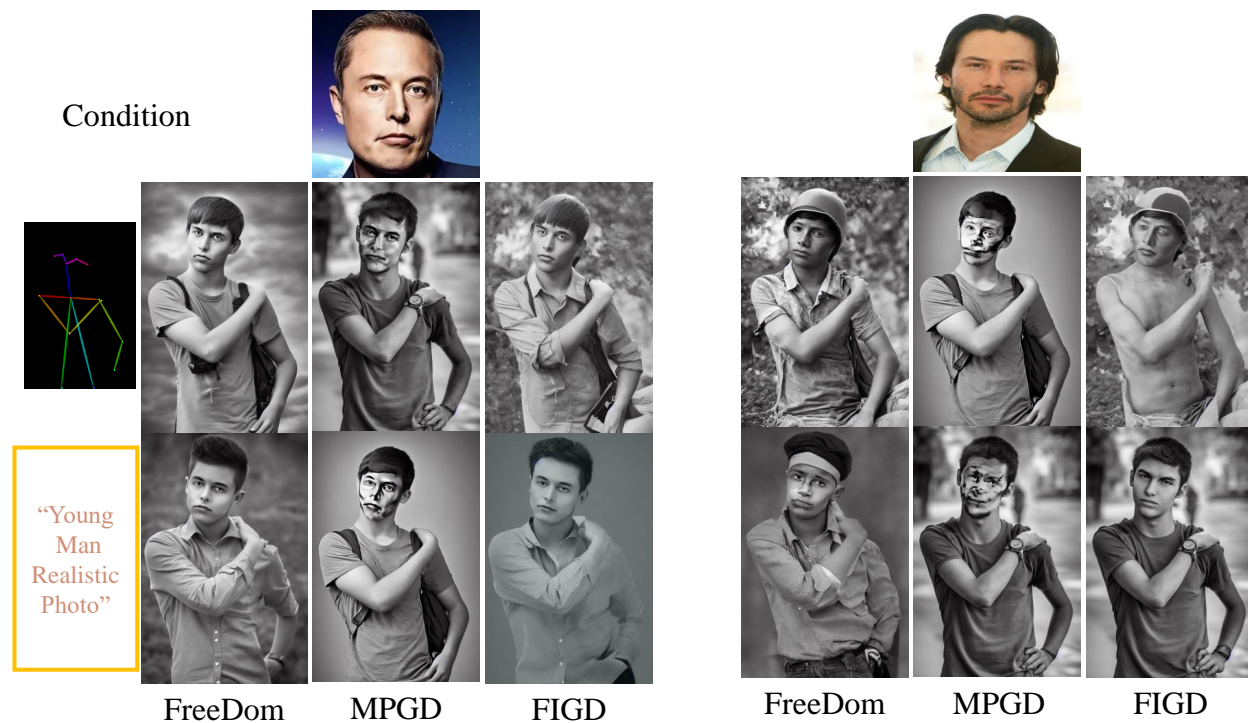


Figure 17: Qualitative examples of face related tasks based on ControlNet experiments. We compared FIGD ( $T = 100$ ) with the FreeDom ( $T = 100$ ) and MPGD ( $T = 100$ ).

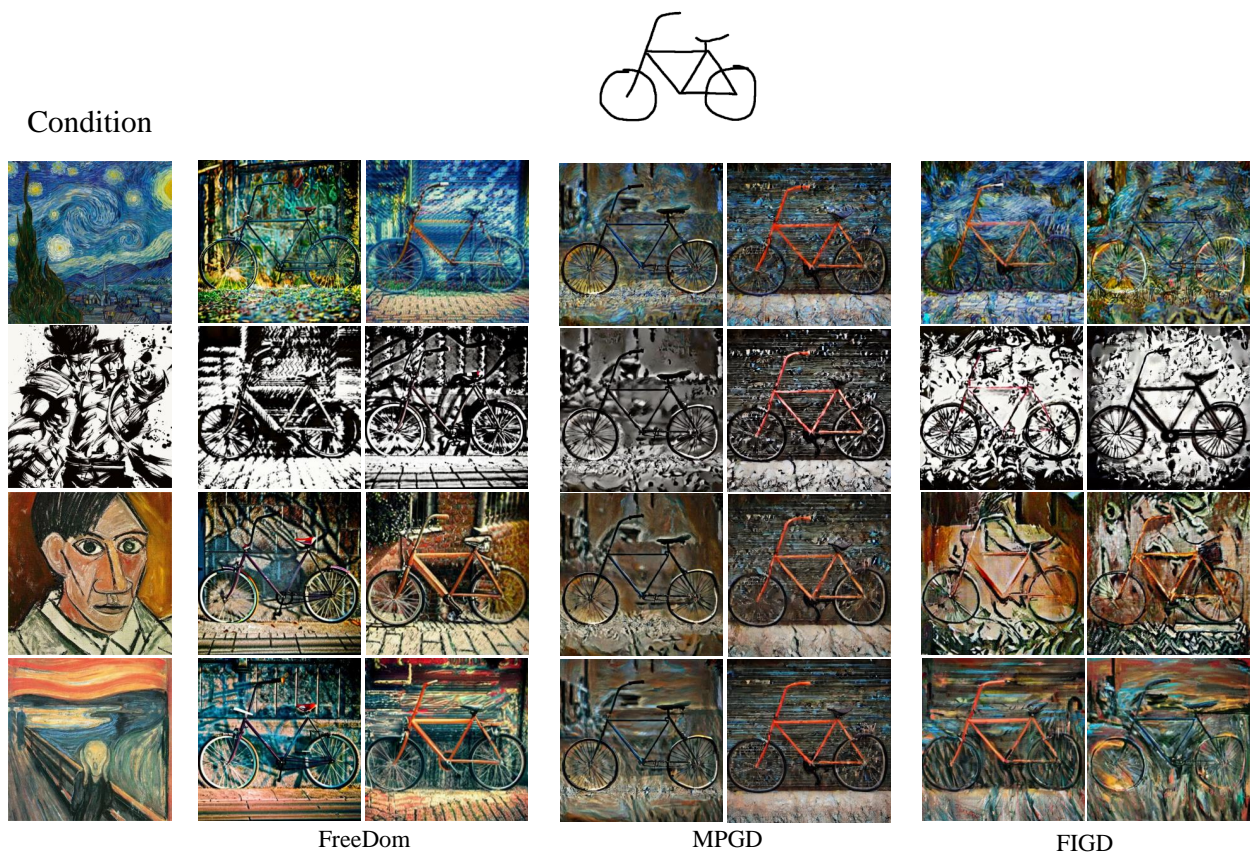


Figure 18: Qualitative examples of style tasks based on ControlNet experiments. We compared FIGD ( $T = 100$ ) with the FreeDom ( $T = 100$ ) and MPGD ( $T = 100$ ).

Condition

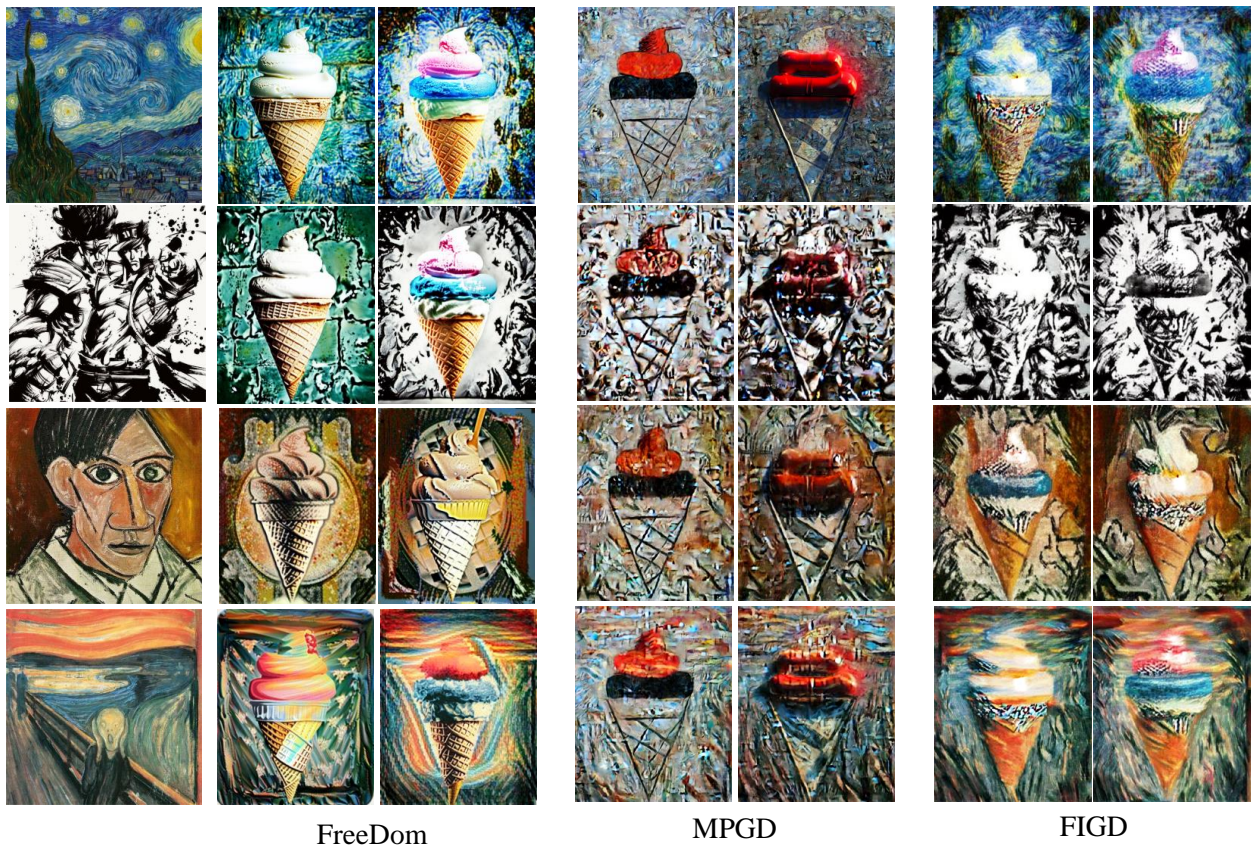
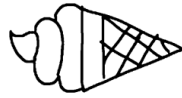


Figure 19: Qualitative examples of style tasks based on ControlNet experiments. We compared FIGD ( $T = 100$ ) with the FreeDom ( $T = 100$ ) and MPGD ( $T = 100$ ).

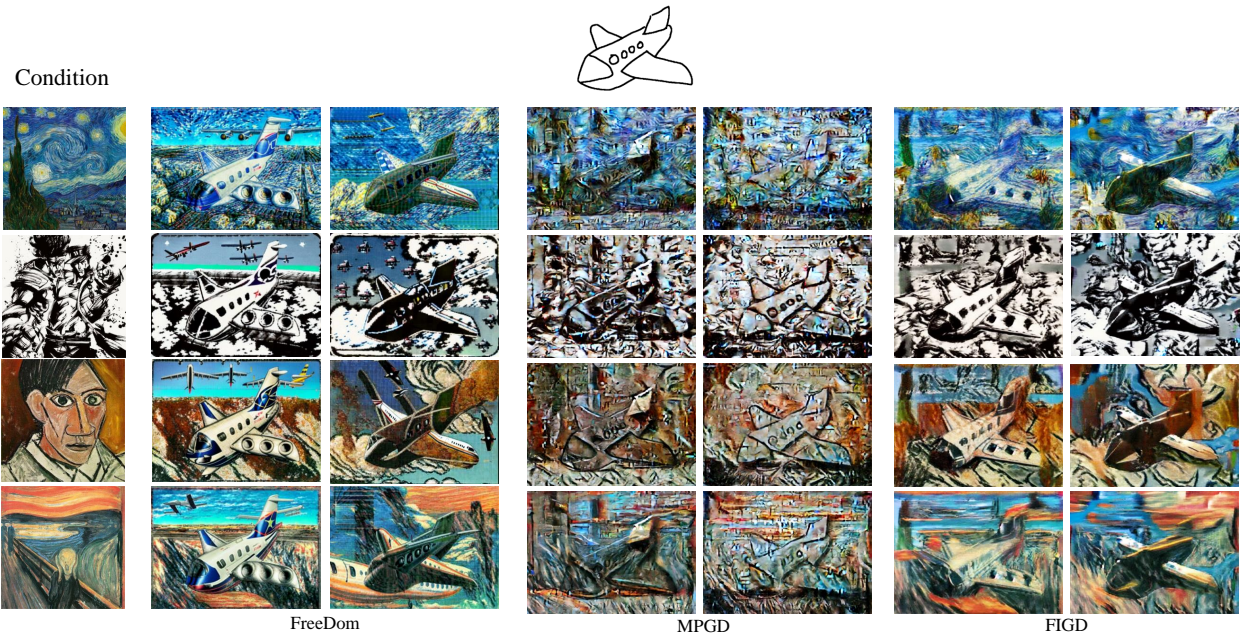


Figure 20: Qualitative examples of style tasks based on ControlNet experiments. We compared FIGD ( $T = 100$ ) with the FreeDom ( $T = 100$ ) and MPGD ( $T = 100$ ).

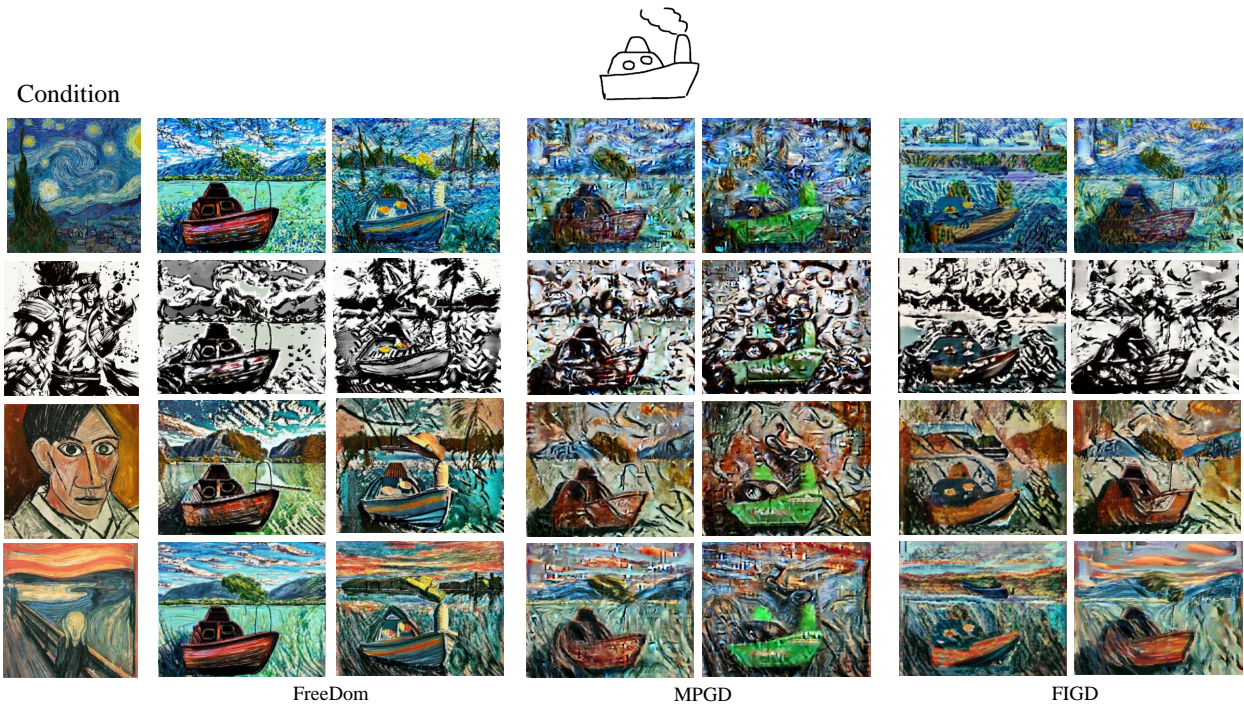


Figure 21: Qualitative examples of style tasks based on ControlNet experiments. We compared FIGD ( $T = 100$ ) with the FreeDom ( $T = 100$ ) and MPGD ( $T = 100$ ).



Figure 22: More qualitative examples of training-free style guidance for FIGD ( $T = 100$ ), where the prompt is "a cat wearing glasses".



Figure 23: More qualitative examples of training-free style guidance for FIGD ( $T = 100$ ), where the prompt is "a cat wearing glasses".

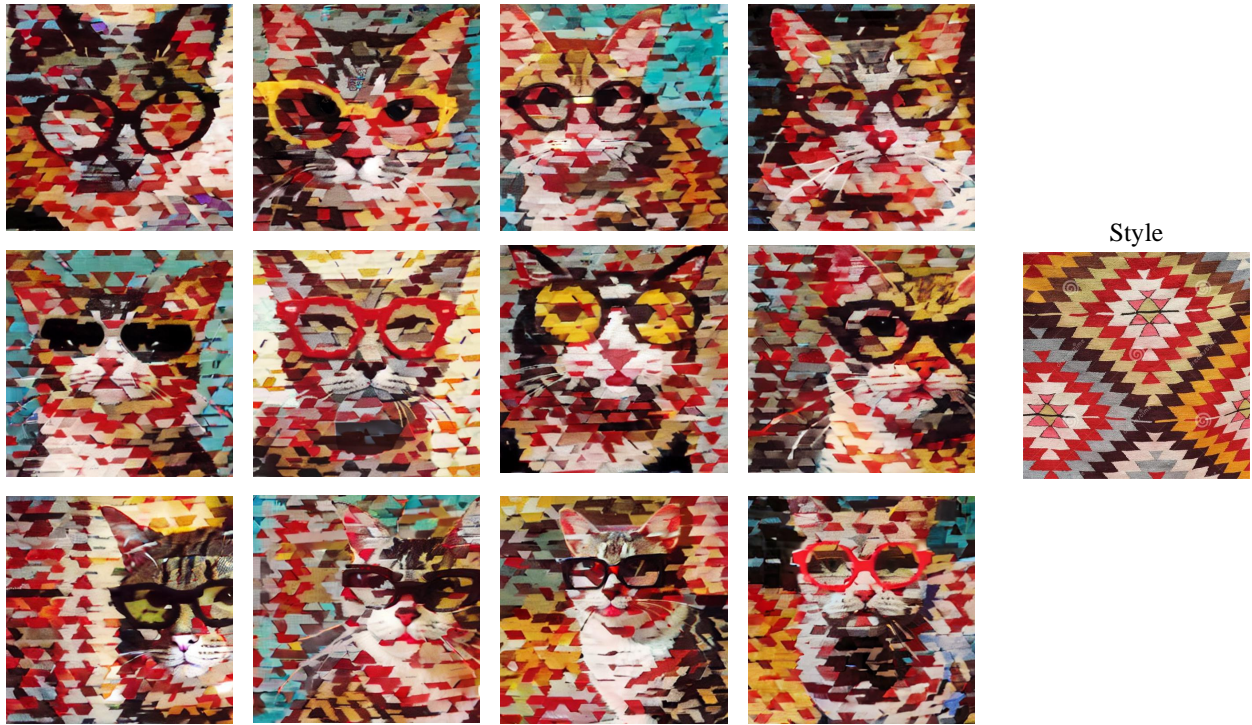


Figure 24: More qualitative examples of training-free style guidance for FIGD ( $T = 100$ ), where the prompt is "a cat wearing glasses".



Figure 25: More qualitative examples of training-free style guidance for FIGD ( $T = 100$ ), where the prompt is "a cat wearing glasses".

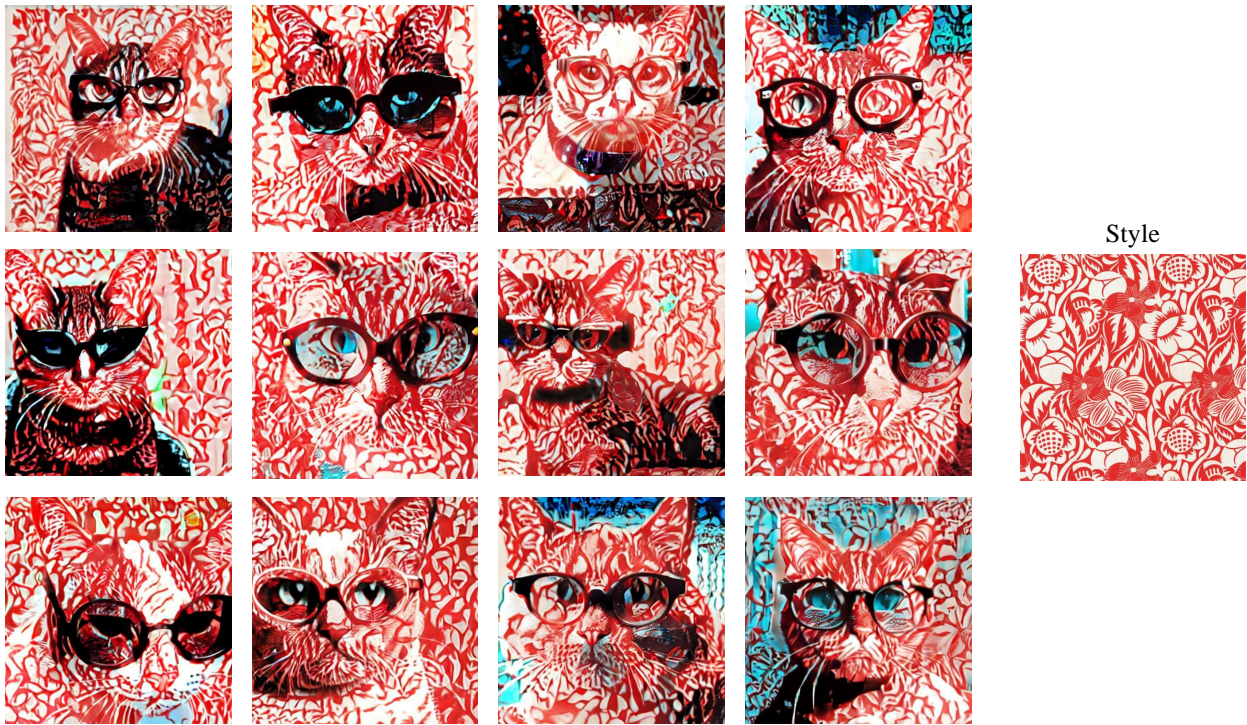


Figure 26: More qualitative examples of training-free style guidance for FIGD ( $T = 100$ ), where the prompt is "a cat wearing glasses".